(Preprint) AAS 19-415

SRP-BASED ORBIT CONTROL WITH APPLICATION TO ORBIT STATIONKEEPING AT SMALL BODIES

Kenshiro Oguri* **and Jay W. McMahon†**

With appropriate control algorithms, solar radiation pressure (SRP) can be effectively exploited as a source of orbit control force around asteroids. A concept of SRP-based orbit control utilizes the SRP acceleration for controlling spacecraft orbits by *active* attitude changes, for which the authors recently developed an optimal control law with an asteroid landing scenario. In contrast to a hypothetical spacecraft assumed in the landing scenario, common spacecrafts usually have lower area-to-mass ratios as well as attitude constraints such as a constraint on the maximum pitch angle of spacecraft solar panels against the sunlight. Extending the concept to such common spacecrafts requires careful design of a feedback control gain associated with the control law. This paper introduces a state-dependent feedback gain for the control law and demonstrates the controller's capability with two scenarios inspired by the OSIRIS-REx science planning: 1) orbit stationkeeping at science orbits and 2) orbit transfer in-between.

INTRODUCTION

Historically, solar radiation pressure (SRP) has been treated as one of primary disturbances affecting spacecraft dynamics around asteroids. While other perturbations such as the irregular gravity field of the primary body and the gravitational attraction from the Sun also influence the dynamics, SRP is likely to be the dominant perturbation around asteroids with radii of less than several kilometers.[1] SRP is, however, also an important source of orbit control force. SRP acceleration can be controlled by changing spacecraft attitude whereas most of other perturbations cannot be. Furthermore, at the asteroids' weak gravity environment, the SRP-based orbit control can provide a considerable control authority, enabling effective, fuel-free orbit control.

Many studies have investigated orbital dynamics around asteroids under the strong influence of SRP. They have found several types of stable orbits, including terminator orbits,[1–4] quasi-terminator orbits,[5] heliotropic orbits,[6,7] and delta-V assisted periodic orbits.[8] These studies regard the orbital dynamics as *decoupled* from the attitude (i.e., assuming the cannon ball model). Some other studies discuss the attitude-orbit coupled dynamics around asteroids, including hovering and orbiting operation,[9] relative pose estimation,[10] hovering over elongated asteroids,[11] periodic orbits around artificial equilibrium points in binary asteroid systems,[12] and passive stability of both terminator orbits and sun-tracking attitude motion.[13] As a new approach, the authors of this paper recently developed an SRP-based orbit control law so that the SRP acceleration can be effectively exploited via *active* attitude control.[14] With the control law, the authors demonstrated the concept with an

*Ph.D. student, Graduate Research Assistant, Colorado Center for Astrodynamics Research, Department of Aerospace Engineering Sciences, UCB, Boulder, CO 80309.

†Assistant Professor, Colorado Center for Astrodynamics Research, Department of Aerospace Engineering Sciences, UCB, Boulder, CO 80309.

asteroid landing scenario for future asteroid exploration. All the studies provide insight into the orbital dynamics around asteroids influenced by SRP with constant and/or passive spacecraft attitude or its active control.

To extend the SRP-based orbit control concept to common (or traditional) asteroid explorers such as OSIRIS-REx[15] and Hayabusa[16] spacecrafts, further efforts are required. While the landing scenario assumed a hypothetical spacecraft with a relatively high area-to-mass ratio ($\sim$ 0.1-1.0 $[\mathrm{m}^2/\mathrm{kg}]$) and no attitude constraints, common spacecrafts usually have lower area-to-mass ratios ($\sim$ 0.01-0.05 $[\mathrm{m}^2/\mathrm{kg}]$) and attitude constraints for sufficient power generation. These properties of common spacecrafts comparatively decrease the orbit control capability by SRP. Given such considerations associated with common spacecrafts, seeking improvement of the controller performance is critical to make the SRP-based orbit control concept an available option for future asteroid missions.

In aim to improve the controller performance, the present paper introduces a state-dependent feedback control gain to the SRP-based orbit control concept. Since the control law provides an optimal control input (i.e., attitude angle) based on a feedback gain, the gain governs the controller behavior; a choice of the gain significantly affects the performance especially when the orbit control capability by SRP is very small relative to the natural dynamics. Scenarios considered in this paper fall into such cases. The state-dependent gain is inspired by the Q-law,[17–19] which was originally developed for low-thrust orbit transfers. With the newly introduced gain, the SRP-based orbit controller is tested with two scenarios inspired by the OSIRIS-REx science planning: 1) orbit stationkeeping at science orbits and 2) orbit transfer in-between. The two scenarios are demonstrated with numerical simulations that include dynamical disturbances of SRP, solar gravity, and irregular gravity field (16×16) of Bennu.

DYNAMICS

Coordinate frame

This paper employs three coordinate frames: Asteroid-Centered Hill (ACH) frame, Asteroid-Centered Asteroid-Fixed frame (ACAF) frame, and Spacecraft-Centered Hill (SCH) frame. Each frame is illustrated in Figures 1 and 2. The origin of the ACH frame is fixed at the asteroid's center of mass and $\hat{\boldsymbol{x}}^{\mathrm{ACH}}$ is aligned with the sun-asteroid vector, $\hat{\boldsymbol{z}}^{\mathrm{ACH}}$ is aligned with the angular momentum of the asteroid about the Sun, and $\hat{\boldsymbol{y}}^{\mathrm{ACH}}$ is in the orbit plane and forms a right-hand system. The origin of the ACAF frame is fixed at the asteroid and rotates with it, where asteroid rotation rate is assumed constant about $\hat{\boldsymbol{z}}^{\mathrm{ACAF}}$, assuming a principal axis rotator. The SCH frame has its origin at the spacecraft center of mass, moves with the spacecraft orbit about the asteroid, and consists of $\hat{\boldsymbol{r}}, \hat{\boldsymbol{\theta}}, \hat{\boldsymbol{H}}$, where $\hat{\boldsymbol{r}}$ is aligned with the asteroid-spacecraft vector, $\hat{\boldsymbol{H}}$ is aligned with the angular momentum of the spacecraft orbit about the asteroid, and $\hat{\boldsymbol{\theta}}$ is in the orbit plane and forms a right-hand system.

Spacecraft attitude is defined with respect to each axis of the ACH frame by two angles: pitch angle α and clock angle β. Figure 2(b) illustrates the spacecraft attitude in the ACH frame. Since we consider the spacecraft motion in the proximity of an asteroid, we assume the sun-spacecraft vector $\hat{\boldsymbol{s}}$ is aligned to the sun-asteroid vector $\hat{\boldsymbol{x}}^{\mathrm{ACH}}$. The attitude angles compose the control input as $\boldsymbol{u} = [\alpha, \beta]^T \in \mathcal{U} \subset \mathbb{R}^2$, where $\mathcal{U} = \{\alpha, \beta : 0 \leq \alpha \leq \pi/2, 0 \leq \beta \leq 2\pi\}$.

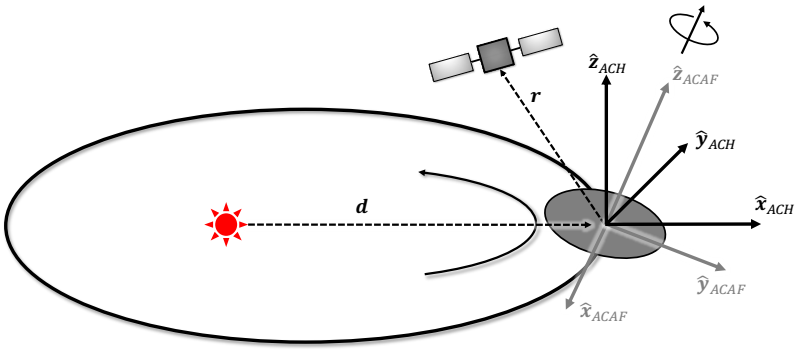

Figure 1. Asteroid-Centered Hill (ACH) and Asteroid-Centered Asteroid-Fixed (ACAF) frames.

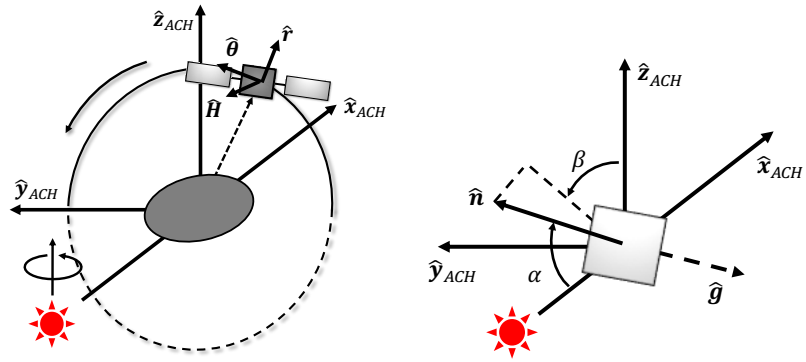

(a) Spacecraft-Centered Hill (SCH) frame. (b) Attitude definition

Figure 2. Spacecraft-Centered Hill (SCH) frame and attitude definition.

SRP force model

This paper expresses SRP force based on *optical force model*,[20–22] which takes into account the combined contributions of specular and diffusive reflection, absorption, and emission of radiation on spacecraft surface. We use $\rho \in [0,1]$ for the total reflectivity, $s \in [0,1]$ for specular ratio, $B_L = 2/3$ for diffusive reflection coefficient assuming Lambertian surface, and ϵ_f, ϵ_b for front and back surface emission coefficients. With the sunlight vector $\hat{\boldsymbol{s}}$, the vector normal to the surface $\hat{\boldsymbol{n}}$, and the pitch angle α, which are defined in Figure 3, each term of the SRP force acting on a differential area are expressed as

$$\begin{aligned} \boldsymbol{g} =& \boldsymbol{F}_{\mathrm{SRP}}/m = g_0\, \hat{\boldsymbol{g}}, \\ g_0 =& \sigma P(d),\ \hat{\boldsymbol{g}} = -(C_1 \cos^2\alpha + C_2 \cos\alpha)\hat{\boldsymbol{n}} + C_3 \cos\alpha \hat{\boldsymbol{s}}, \end{aligned} \tag{1}$$

where the term $\sigma = A/m[\mathrm{m}^2/\mathrm{kg}]$ is spacecraft area/mass ratio, $P(d) = \frac{E_{\mathrm{E}} d_{\mathrm{E}}^2}{c\, d^2}$ is the magnitude of SRP acting on a unit area at the solar distance $d = |\boldsymbol{d}|$, and $E_{\mathrm{E}} = 1.366 \times 10^3 [\mathrm{W/m}^2], c = 2.998 \times 10^8 [\mathrm{m/s}], d_{\mathrm{E}} = 1.496 \times 10^{11} [\mathrm{m}]$ are the solar constant at Earth, speed of the light, and the Sun-Earth distance, respectively. C_1, C_2, C_3 are defined as

$$C_1 = 2\bar{\rho}\bar{s},\ C_2 = B_L\bar{\rho}(1-\bar{s}) + \frac{B_L(\bar{\epsilon_f} - \bar{\epsilon_b})}{\bar{\epsilon_f} + \bar{\epsilon_b}},\ C_3 = 1 - \bar{\rho}\bar{s}. \tag{2}$$

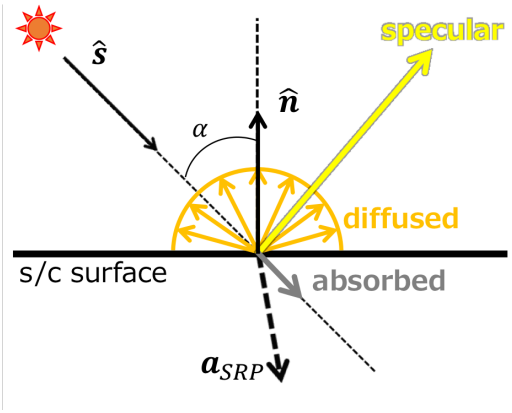

Figure 3. SRP reflection on spacecraft surface.

In the ACH frame, as $\hat{\boldsymbol{n}}^{\mathrm{ACH}} = [-\cos\alpha,\ \sin\alpha\sin\beta,\ \sin\alpha\cos\beta]^T$ and $\hat{\boldsymbol{s}}^{\mathrm{ACH}} = [1,\ 0,\ 0]^T$, $\boldsymbol{g}^{\mathrm{ACH}} = [g_x, g_y, g_z]^T$ is

$$\boldsymbol{g}^{\mathrm{ACH}} = g_0 \cos\alpha \begin{bmatrix} C_1\cos^2\alpha + C_2\cos\alpha + C_3 \\ -(C_1\cos\alpha + C_2)\sin\alpha\sin\beta \\ -(C_1\cos\alpha + C_2)\sin\alpha\cos\beta \end{bmatrix}. \tag{3}$$

Note that λ is expressed as

$$\tan\lambda = \frac{\sqrt{g_y^{\mathrm{ACH}^2} + g_z^{\mathrm{ACH}^2}}}{g_x^{\mathrm{ACH}}} = \frac{(C_1\cos\alpha + C_2)\sin\alpha}{C_1\cos^2\alpha + C_2\cos\alpha + C_3}. \tag{4}$$

Equations of motion

Throughout this paper, orbital dynamics of spacecraft is considered in the vicinity of an asteroid, i.e., two-body problem (asteroid and spacecraft) with perturbations. Let the perturbing acceleration $\boldsymbol{a}$ be $\boldsymbol{a} = \boldsymbol{\xi}(\boldsymbol{x}) + \boldsymbol{g}(\boldsymbol{x}, \boldsymbol{u})$, where $\boldsymbol{\xi}$ is a sum of perturbations that only depend on spacecraft position (e.g., the solar gravity and the irregular gravity field). Recall that the vector $\boldsymbol{u} = [\alpha, \beta]^T$ represents spacecraft attitude.

Lagrange's planetary equations in the Gauss form are used in this paper to express the dynamics as they explicitly describe the effect of perturbations on the two-body dynamics. Let the state vector be $\boldsymbol{x} = [a, e, i, \omega, \lambda, f]^T$, where $\lambda = \Omega - f_{\mathrm{sb}}$. The equations of motion are then[23]

$$\dot{\boldsymbol{x}} = \boldsymbol{n}^{\mathrm{ACH}} + B^{\mathrm{ACH}}\boldsymbol{a}^{\mathrm{ACH}}, \tag{5}$$

where

$$\boldsymbol{n}^{\mathrm{ACH}} = \begin{bmatrix} 0 & 0 & 0 & 0 & -\dot{f}_{\mathrm{sb}} & \sqrt{\mu/a^3} \end{bmatrix}^T, \quad B^{\mathrm{ACH}} = B^{\mathrm{SCH}} T_{\mathrm{SCH}}^{\mathrm{ACH}},$$

$$B^{\mathrm{SCH}} = \frac{1}{\sqrt{\mu}} \begin{bmatrix} \dfrac{2a^{3/2} e \sin f}{\sqrt{1-e^2}} & \dfrac{2a^{3/2}(1+e\cos f)}{\sqrt{1-e^2}} & 0 \\ \sqrt{a(1-e^2)}\sin f & \sqrt{a(1-e^2)}\left(\dfrac{e+\cos f}{1+e\cos f} + \cos f\right) & 0 \\ 0 & 0 & \dfrac{\sqrt{a(1-e^2)}\cos\theta}{1+e\cos f} \\ -\dfrac{\sqrt{a(1-e^2)}\cos f}{e} & \dfrac{\sqrt{a(1-e^2)}(2+e\cos f)\sin f}{e(1+e\cos f)} & -\dfrac{\sqrt{a(1-e^2)}}{\tan i}\dfrac{\sin\theta}{1+e\cos f} \\ 0 & 0 & \dfrac{\sqrt{a(1-e^2)}}{\sin i}\dfrac{\sin\theta}{1+e\cos f} \\ \dfrac{\sqrt{a(1-e^2)}\cos f}{e} & -\dfrac{\sqrt{a(1-e^2)}(2+e\cos f)\sin f}{e(1+e\cos f)} & 0 \end{bmatrix}. \tag{6}$$

Note that $\theta = \omega + f$, $T_{\mathrm{ACH}}^{\mathrm{SCH}}$ denotes the coordinate transformation from the ACH to SCH frame, and $\boldsymbol{a}^{\mathrm{ACH}}$ is perturbing acceleration in the ACH frame.

SRP-BASED ORBIT CONTROL

Lyapunov feedback controller

The authors previously developed an optimal feedback controller for the SRP-based orbit control.[14] The controller provides a closed-form solution that minimize the time derivative of a Lyapunov function $V = \frac{1}{2}\delta\boldsymbol{x}^T K \delta\boldsymbol{x}$, which represents a *state distance* weighted by a matrix $K \in \mathbb{R}^{n\times n}$. $\delta\boldsymbol{x} = \boldsymbol{x} - \boldsymbol{x}_r$ is a difference in osculating orbital elements between the current and target (reference) orbits. Since the matrix K defines the Lyapunov function V, it must be positive semi-definite ($K \succeq 0$) and can be regarded as a feedback gain that dictates how the feedback control is performed.

Here the derivation of the controller is briefly reviewed for convenience. The optimal control problem is formulated as

$$\begin{aligned} \boldsymbol{u}^* &= \arg\min_{\boldsymbol{u}\in\mathcal{U}} J, \\ J &= \frac{dV}{dt} = \delta\boldsymbol{x}^T K \dot{\boldsymbol{x}} = \delta\boldsymbol{x}^T K B^{\mathrm{ACH}} \boldsymbol{a}^{\mathrm{ACH}} = -\boldsymbol{\chi}^T \cdot [\boldsymbol{g}^{\mathrm{ACH}}(\boldsymbol{x},\boldsymbol{u}) + \boldsymbol{\xi}^{\mathrm{ACH}}(\boldsymbol{x})], \end{aligned} \tag{7}$$

where $\boldsymbol{\chi}^T \triangleq -\delta\boldsymbol{x}^T K B^{\mathrm{ACH}}$. Note that $\boldsymbol{\chi}$ is equivalent to $\boldsymbol{\Delta}$ in the original literature (modified to avoid potential confusions with the Laplace operator and/or with the increment operator). Let us write $\boldsymbol{\chi} = [\chi_x, \chi_y, \chi_z]^T$ to express $\boldsymbol{\chi} \in \mathbb{R}^{3\times 1}$ in the ACH frame. Finding the optimal feedback control $\boldsymbol{u}^* (= [\alpha^*, \beta^*]^T)$ is equivalent to solving

$$\boldsymbol{u}^* = \arg_{\boldsymbol{u}\in\mathcal{U}} \left[\frac{\partial J}{\partial \boldsymbol{u}} = \boldsymbol{0}_{1\times 2} \ \wedge \ \frac{\partial^2 J}{\partial \boldsymbol{u}^2} \succeq 0 \right]. \tag{8}$$

As derived in Reference 14, the optimal control problem is solved to yield:

$$
\begin{aligned}
\alpha^* =& \alpha_0 - \frac{\mathcal{F}(\alpha_0)}{\mathcal{F}_\alpha(\alpha_0)}, \\
\mathcal{F}(\alpha) =& -k[3C_1\cos^2\alpha + 2C_2\cos\alpha + C_3]\sin\alpha + C_1\cos\alpha(1-3\sin^2\alpha) + C_2\cos 2\alpha, \\
\mathcal{F}_\alpha(\alpha) =& -k\left[3C_1(\cos^3\alpha - 2\cos\alpha\sin^2\alpha) + 2C_2\cos 2\alpha + C_3\cos\alpha\right] + C_1\sin\alpha(2-9\cos^2\alpha) - 2C_2\sin 2\alpha, \\
\alpha_0 =& \arctan\left[\frac{1}{4}\left(-3k + \sqrt{8+9k^2}\right)\right], \quad k = \frac{\chi_x}{\sqrt{\chi_y^2+\chi_z^2}}, \\
\beta^* =& \arctan 2(-\chi_y, -\chi_z),
\end{aligned}
\tag{9}
$$

where α_0 is the optimal pitch angle for the control problem under a simplified SRP reflection model (see Reference 14 for more detail).

State-dependent gain for Lyapunov feedback control

The SRP-based orbit control law has a free parameter: the feedback gain matrix K, which actually significantly affects the controller performance. While the gain matrix is left constant in the previous applications to landing scenarios, where a high area-to-mass ratio spacecraft is assumed, choosing appropriate gains becomes critical when considering orbit control with common spacecraft (less area-to-mass ratio). In fact, as discussed in the "Numerical simulations" section, just choosing a constant feedback gain ($K = I_5$) is not effective, making it unreliable to perform intended orbit controls.

Adaptively changing the feedback gain depending on the current state is expected to improve the control performance. Since the control influence matrix B^{SCH} is a function of orbital elements, and so is the feedback control input $\boldsymbol{u}^*$ through $\boldsymbol{\chi}$, controllability of each orbital element depends on the current osculating orbital elements (e.g., the orbit inclination cannot be controlled when $\theta = \pi/2$ from Eq. 6).

It is however not trivial to tune K so that provides the "best" performance; we hence take a heuristic approach to the gain tuning problem. Our approach is inspired by the Q-law,[17–19] which was originally developed for low-thrust orbit transfers under the Keplerian dynamics.

Re-formulating our SRP-based orbit control law into a form with a state-dependent feedback gain (denoted by $\widehat{K}$) is straightforward thanks to its originally generic form (except for deriving an optimal $\dot{\widetilde{x}}_i$, as discussed later). Let us rewrite our Lyapunov function V as

$$
V = \frac{1}{2}\widehat{\boldsymbol{x}}^T K \widehat{\boldsymbol{x}}, \quad K = (1+W_p P)\mathrm{diag}([W_1 S_a, W_2, ..., W_5]) \in \mathbb{R}^{5\times 5}, \tag{10}
$$

where

$$
\begin{aligned}
\widehat{\boldsymbol{x}} =& [\widehat{x}_1, \widehat{x}_1, ..., \widehat{x}_5]^T, \quad \widehat{x}_i = \frac{d(x_i, x_{i_r})}{\dot{\widetilde{x}}_i}, \quad d(x_i, x_{i_r}) = \begin{cases} x_i - x_{i_r} & (x_i = a, e, i), \\ \cos^{-1}\left[\cos\left(x_i - x_{i_r}\right)\right] & (x_i = \omega, \Omega), \end{cases} \\
P =& \exp\left[k\left(1 - \frac{a(1-e)}{r_{p\,\min}}\right)\right], \quad S_a = \left[1 + \left(\frac{a-a_r}{m a_r}\right)^n\right]^{1/r}.
\end{aligned}
\tag{11}
$$

In this formulation, V corresponds the "proximity quotient Q" in the original literature and represents "best-case quadratic time-to-go."[19] Note that $r_{p\min}$ is a minimum allowable periapsis radius and $W_P, W_1, W_2, ..., W_5, m(=3), n(=4), r(=2)$ are scalar design parameters, where inside the parentheses are the values used in the original literature on the Q-law. P is a penalty function that increases the V value when the state is close to the primary body with an exponential barrier. $\dot{\tilde{x}}_i$ is defined as

$$\dot{\tilde{x}}_i = \max_{\alpha,\beta,f} \dot{x}_i = \max_f \left[\boldsymbol{n}^{\mathrm{ACH}} + B^{\mathrm{ACH}}(\boldsymbol{g}^{\mathrm{ACH}}(\alpha^*, \beta^*) + \boldsymbol{\xi}^{\mathrm{ACH}}) \right]_i, \tag{12}$$

where $\boldsymbol{g}^{\mathrm{ACH}}$ and $\{\alpha^*, \beta^*\}$ are as defined/obtained in Eqs. 3 and 9, respectively. Then the time derivative of the Lyapunov function V is $J = \frac{dV}{dt} = \widehat{\boldsymbol{x}}^T K \dot{\widehat{\boldsymbol{x}}} + \frac{1}{2}\widehat{\boldsymbol{x}}^T \dot{K} \widehat{\boldsymbol{x}}$, where

$$\begin{aligned} \dot{\widehat{\boldsymbol{x}}} =& \mathrm{diag}\left(\left[\frac{\partial \widehat{x}_1}{\partial x_1}, \frac{\partial \widehat{x}_2}{\partial x_2}, ..., \frac{\partial \widehat{x}_5}{\partial x_5} \right] \right) \dot{\boldsymbol{x}}, \\ \dot{K}\widehat{\boldsymbol{x}} =& \left[\sum_i \frac{\partial K}{\partial x_i} \dot{x}_i \right] \widehat{\boldsymbol{x}} = \left[\sum_i \frac{\partial K}{\partial x_i} \widehat{\boldsymbol{x}} \dot{x}_i \right] = \left[\frac{\partial K}{\partial x_1}\widehat{\boldsymbol{x}} \quad \frac{\partial K}{\partial x_2}\widehat{\boldsymbol{x}} \quad \cdots \quad \frac{\partial K}{\partial x_5}\widehat{\boldsymbol{x}} \right] \dot{\boldsymbol{x}}. \end{aligned} \tag{13}$$

Thus we have

$$J = \widehat{\boldsymbol{x}}^T \widehat{K} \dot{\boldsymbol{x}}, \quad \widehat{K} \triangleq K \cdot \mathrm{diag}\left(\left[\frac{\partial \widehat{x}_1}{\partial x_1}, \frac{\partial \widehat{x}_2}{\partial x_2}, ..., \frac{\partial \widehat{x}_5}{\partial x_5} \right] \right) + \frac{1}{2} \left[\frac{\partial K}{\partial x_1}\widehat{\boldsymbol{x}} \quad \frac{\partial K}{\partial x_2}\widehat{\boldsymbol{x}} \quad \cdots \quad \frac{\partial K}{\partial x_5}\widehat{\boldsymbol{x}} \right], \tag{14}$$

where

$$\begin{aligned} \frac{\partial \widehat{x}_i}{\partial x_i} =& \frac{1}{\dot{\tilde{x}}} - \frac{d(x_i, x_{i_r})}{\dot{\tilde{x}}_i^2} \frac{\partial \dot{\tilde{x}}_i}{\partial x_i}, \\ \frac{\partial K}{\partial x_i} =& W_P \frac{\partial P}{\partial x_i} \mathrm{diag}([W_1 S_a, W_2, ..., W_5]) + (1 + W_P P) \mathrm{diag}\left(\left[W_1 \frac{\partial S_a}{\partial x_i}, 0, ..., 0 \right] \right), \\ \frac{\partial P}{\partial x_i} =& \begin{cases} -k(1-e^2)\left(1 - \dfrac{r_p}{r_{p\min}}\right) \exp\left[k\left(1 - \dfrac{r_p}{r_{p\min}}\right)\right], & (x_i = a) \\ 2kae\left(1 - \dfrac{r_p}{r_{p\min}}\right) \exp\left[k\left(1 - \dfrac{r_p}{r_{p\min}}\right)\right], & (x_i = e) \\ 0, & (x_i = i, \omega, \Omega) \end{cases} \\ \frac{\partial S_a}{\partial x_i} =& \frac{n}{r}\left[1 + \left(\frac{a - a_r}{m a_r} \right)^n \right]^{\frac{1}{r}-1} \left(\frac{a - a_r}{m a_r} \right)^{n-1}, \end{aligned} \tag{15}$$

which implies that Eq. 9 is directly applicable with only one change in the solution form. That is, we can use Eq. 9 as it is with a replacement of $\boldsymbol{\chi}$ with the following new $\boldsymbol{\chi}$, denoted by $\boldsymbol{\chi}_Q$:

$$\boldsymbol{\chi}_Q^T = -\hat{\boldsymbol{x}}^T \hat{K} B^{\mathrm{ACH}}. \tag{16}$$

Obtaining an explicit form of $\dot{\tilde{x}}_i$ is however not straightforward for the SRP-based orbit control. It requires finding an appropriate true anomaly f that maximizes the i-th component of

$$\dot{\boldsymbol{x}} = \boldsymbol{n}^{\mathrm{ACH}} + B^{\mathrm{ACH}}(\boldsymbol{g}^{\mathrm{ACH}}(\alpha^*, \beta^*) + \boldsymbol{\xi}^{\mathrm{ACH}}). \tag{17}$$

In order to obtain $\dot{\widetilde{x}}_1 = \dot{\widetilde{a}}$ for example, even if we assume the simplest dynamics, i.e., the Keplerian (plus SRP) dynamics with the ideal reflection model ($C_1 = 2, C_2 = C_3 = 0$) and no maximum pitch angle constraint ($\alpha \in [0, \pi/2]$), we need to solve the following laboursome equation:

$$\dot{\widetilde{a}} = \max_f \left[2g_0 \cos^2\alpha^* \boldsymbol{b}_a^{\mathrm{SCH}^T} T_{\mathrm{SCH}}^{\mathrm{ACH}} \begin{bmatrix} \cos\alpha^* \\ -\sin\alpha^* \sin\beta^* \\ -\sin\alpha^* \cos\beta^* \end{bmatrix} \right],$$

$$\text{s.t.} \quad \begin{cases} \boldsymbol{b}_a^{\mathrm{SCH}^T} &= \begin{bmatrix} \dfrac{2a^{3/2} e \sin f}{\sqrt{1-e^2}} & \dfrac{2a^{3/2}(1+e\cos f)}{\sqrt{1-e^2}} & 0 \end{bmatrix}, \\ T_{\mathrm{SCH}}^{\mathrm{ACH}} &= \mathrm{Rot}_3[\theta]\mathrm{Rot}_1[i]\mathrm{Rot}_3[\Omega], \\ \alpha^* &= \arctan\left[\dfrac{1}{4}\left(-3k + \sqrt{8+9k^2}\right)\right], \quad k = \dfrac{\chi_x}{\sqrt{\chi_y^2 + \chi_z^2}}, \\ \beta^* &= \arctan 2(-\chi_y, -\chi_z), \quad \boldsymbol{\chi}^T = -(a - a_r)\boldsymbol{b}_a^{\mathrm{SCH}} T_{\mathrm{SCH}}^{\mathrm{ACH}}. \end{cases} \tag{18}$$

Instead, a set of formulations for low-thrust transfer problems provided in Reference 19 is used for now, although it is not optimal for SRP-based orbit control problems. They are summarized in the following for convenience (with some notational changes for consistency):

$$\begin{aligned} \dot{\widetilde{x}}_1 =& \dot{\widetilde{a}} = 2g_0 \sqrt{\frac{a^3(1+e)}{\mu(1-e)}}, \\ \dot{\widetilde{x}}_2 =& \dot{\widetilde{e}} = 2g_0 \sqrt{\frac{a(1-e^2)}{\mu}}, \\ \dot{\widetilde{x}}_3 =& \dot{\widetilde{i}} = \frac{pg_0}{h(\sqrt{1-e^2\sin^2\omega} - e|\cos\omega|)}, \\ \dot{\widetilde{x}}_4 =& \dot{\widetilde{\omega}} = \frac{\dot{\widetilde{\omega}}_i + b\dot{\widetilde{\omega}}_o}{1+b}, \\ \dot{\widetilde{x}}_5 =& \dot{\widetilde{\Omega}} = \frac{pg_0}{h\sin i(\sqrt{1-e^2\cos^2\omega} - e|\sin\omega|)}, \end{aligned} \tag{19}$$

where $h = \sqrt{\mu p}$ and $p = a(1-e^2)$. Their partials, which are necessary in Eq.15, are also found as

$$\frac{\partial \dot{\widetilde{a}}}{\partial a} = 3g_0 \sqrt{\frac{a(1+e)}{\mu(1-e)}}, \quad \frac{\partial \dot{\widetilde{e}}}{\partial e} = -2g_0 e \sqrt{\frac{a}{\mu(1-e^2)}}, \quad \frac{\partial \dot{\widetilde{i}}}{\partial i} = \frac{\partial \dot{\widetilde{\omega}}}{\partial \omega} = \frac{\partial \dot{\widetilde{\Omega}}}{\partial \Omega} = 0. \tag{20}$$

Deriving better formulations of $\dot{\widetilde{x}}_i$ for the SRP-based orbit control is future work.

NUMERICAL SIMULATIONS

This section presents numerical simulation results of the SRP-based orbit control for: 1) station-keeping control on a frozen terminator orbit with 1.a) a constant feedback gain and 1.b) a state-dependent feedback gain and 2) orbit transfer from one frozen terminator orbit to another with 2.a) nominal spacecraft parameters (similar to the OSIRIS-REx spacecraft) and 2.b) a larger area-to-mass area spacecraft (same value as that of the Hayabusa spacecraft).

Table 1. Characteristic parameters of Bennu[24] and environment model.

$\mu_{\rm sb}[{\rm km}^3/{\rm s}^2]$	$R_{\rm mean}$ [km]	$T_{\rm rotation}$ [h]	$r_{\rm SOI}$ [km]	Ephemeris	Perturbation
4.0×10^{-9}	0.246	4.29	2.620	Horizons database	gravity field (deg. 16, order 16), solar gravity, SRP.

Table 2. Characteristic parameters of spacecraft.

σ [$\rm m^2/kg$]	ρ [$-$]	s [$-$]	(C_1, C_2, C_3) [$-$]	g_0 [$\rm m/s^2$] (at epoch)	$\alpha_{\max}$ [degree]
1/74	0.50	2/3	$(0.667, 0.111, 0.667)$	7.661×10^{-08}	15

Simulation settings

The parameter values used in the all simulations throughout this paper are summarized in Tables 1 (environment) and 2 (spacecraft). The simulation environment uses asteroid Bennu[24] as the primary asteroid. Jan. 1, 2025 is chosen as the epoch of the simulation unless otherwise noted. Note that the maximum allowable pitch angle of the attitude control is set to be 15 degree, which might be a slightly conservative value (orbit controllability will grow if we increase this value), showing the effectiveness of the SRP-based orbit control for orbit stationkeeping and transfer controls with small attitude changes.

The constant gain case uses $K = I_5$, i.e., all orbital elements are controlled with the same gain but its phasing (i.e., true anomaly) is not taken care of. The design parameters used for the state-dependent gain are summarized in Table 3, where $W_p = 0$ is chosen so that the penalty function does not affect the controller. Since the spacecraft is close to the body ($\sim$ 2 km) most time, the penalty function can have undesirable effects on the controller performance. $W_i = 1, \forall i$ means that all the elements except for the true anomaly will be controlled.

Frozen terminator orbit

While frozen terminator orbits have been intensively investigated in the literature (e.g., References 1, 3), a recent study found "better" frozen solutions by taking into account the offset of the orbit center towards the anti-sun direction*. This paper employs the improved frozen orbit as 1) a reference orbit for stationkeeping control and 2) initial and target orbits for transfer control.

Orbital elements and the x-offset of the frozen orbit are calculated as follows. The orbit is defined with respect to a point on the x axis in the ACH frame as its origin (i.e., the origin has an offset in the direction of $\hat{\boldsymbol{x}}^{\rm ACH}$). Given its semi-major axis a_r, the reference eccentricity e_r is obtained from the original frozen condition[3] as:

$$e_r = \cos\Lambda, \quad \tan\Lambda = \frac{3g_0(C_1 + C_2 + C_3)d^2}{2}\sqrt{\frac{a_r}{\mu\mu_{\rm sun}a_{\rm sb}(1-e_{\rm sb}^2)}}, \tag{21}$$

where $\mu_{\rm sun}$ is the gravity parameter of the Sun and the subscript $\square_{\rm sb}$ indicates the orbital elements of the small body's heliocentric orbit. Taking the orbit radius measured from the origin, R_0, at the

*Personal communication with Shota Takahashi. To appear in Reference 25

Table 3. Design parameters for state-dependent feedback gain.

W_p	$[W_1, W_2, W_3, W_4, W_5]$	m	n	r	b	$r_{p\,\min}$
0	$[1, 1, 1, 1, 1]$	3	4	2	0.01	0.283 km

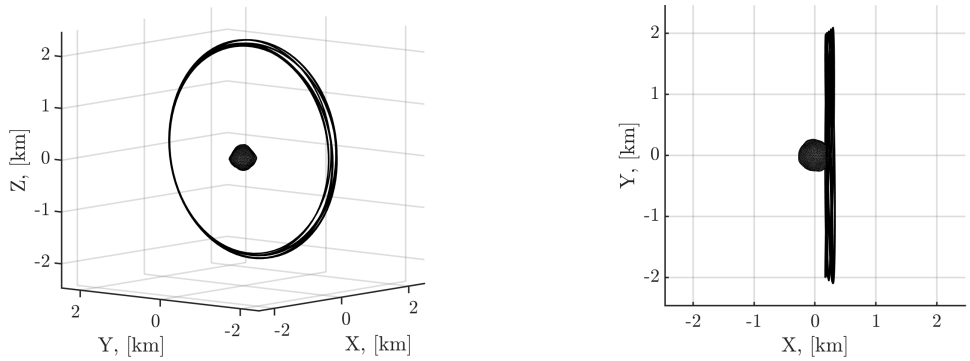

Figure 4. Reference frozen terminator orbit at Bennu designed at the epoch Jan 1 2025, propagated for 30 days. Reference orbital elements are $\{a, e, i, \omega, \Omega\} = \{2.0, 0.0707, \pi/2, -\pi/2, \pi/2\}$ defined with respect to the origin with the x-offset.

periapsis, then $R_0 = a_r(1 - e_r)$. The offset that yields a frozen orbit is then[25]

$$x_{\text{offset}} \approx \frac{R_0^3 g_0 (C_1 + C_2 + C_3)}{\mu} (1 - e_r) \left(1 + \frac{e_r}{4}\right). \tag{22}$$

The reference orbit is designed with the orbit semi-major axis of 2 km (measured from the origin with the offset) at asteroid Bennu at the epoch Jan 1 2025. Reference orbital elements are $\{a, e, i, \omega, \Omega\} = \{2.0, 0.0707, \pi/2, -\pi/2, \pi/2\}$ defined with respect to the origin with the x-offset. Figure 4 shows a trajectory propagated for 30 days taking the reference elements as the initial condition with Bennu's irregular gravity field (16×16), solar gravity, and SRP. Note that the trajectory is not completely same as the reference orbit due to the perturbations.

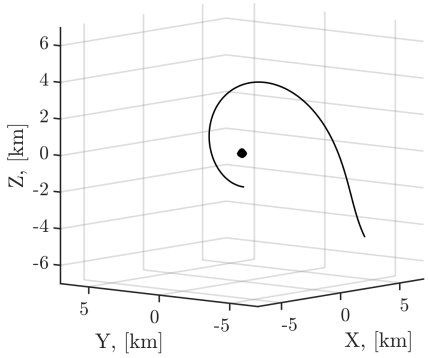

Figure 5. Without any control, spacecraft escaped from the Bennu's gravity field in 8 days, with the initial perturbation of 5 mm/s in its velocity.

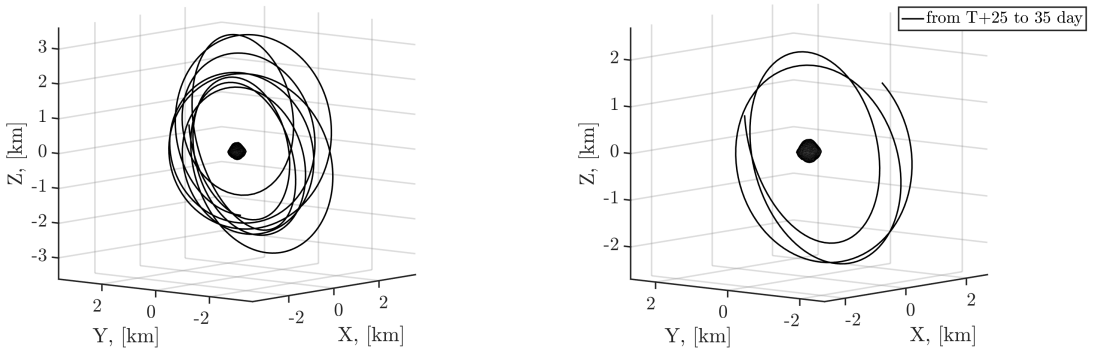

Figure 6. Spacecraft trajectory with stationkeeping control by SRP, with constant gain matrix. Left: from the initial epoch to the end, right: last ten days (to emphasize the final portion of the trajectory). The same initial perturbation as in Figure 5 is added.

Stationkeeping control

Two SRP-based orbit controllers are tested with a stationkeeping control scenario. The controllers are the Lyapunov feedback control with a) constant and b) state-dependent feedback gains. Feedback gain parameters are summarized in the "Simulation settings" subsection.

The stationkeeping scenario assumes that a spacecraft is inserted into a science orbit (frozen terminator orbit) from a higher-altitude orbit with a small perturbation in the initial velocity after the orbit insertion. Even if the velocity error is small, it can be significant enough to let the spacecraft escape from the small body gravity field, which can lead to a mission failure. In practice, clean-up maneuvers are usually planned to cancel out potential errors after the orbit insertion (see References 15, 26 for the OSIRIS-REx mission design for example). Instead, this scenario tries to cancel out the insertion error by the SRP-based orbit control, where the frozen terminator orbit defined in the previous subsection is used as the reference orbit. The tested initial perturbation is $+5$ mm/s velocity in the $\hat{\boldsymbol{y}}^{\mathrm{ACH}}$ direction. It is larger than but in the same order as assumed in a sensitivity analysis of frozen terminator orbits against maneuver errors for the OSIRIS-REx mission,[27] where a 1 mm/s random velocity perturbation is assumed. With the perturbation, the initial orbital elements are $\boldsymbol{x} = [a, e, i, \omega, \Omega]^T = [2.71 \text{ km}, 0.311, 1.46 \text{ rad}, \pi/2 \text{ rad}, \pi/2 \text{ rad}]^T$. Without any active control, the spacecraft escaped from the asteroid gravity field in 8 days, as shown in Figure 5.

The simulation results with the SRP-based orbit control are shown in Figures 6 (constant gain) and 7 (state-dependent gain), where the spacecraft trajectories are shown in the ACH frame. We can see that the both control algorithms successfully prevent the spacecraft from departing the asteroid at least; however, the convergence speed to the reference orbit is largely different from each other. Whereas the trajectory controlled with the constant gain is not converged yet to the reference in 35 days, the control with the state-dependent gain successfully cancels out the velocity perturbation and converges to the reference almost perfectly. The difference can be clearly seen in the right figures in these figures, where the last portions (last 10 days) of the trajectories are shown.

To compare the convergence more intuitively, Figures 8 show time histories of the osculating orbital elements controlled by the two controllers (left: constant gain, right: state-dependent gain). Note that the semi-major axis is scaled by a factor of 3 to concisely illustrate the figures. Even though the constant-gain controller successfully prevents the escape (Figure 5), its convergence to the target orbit is poor. On the other hand, the state-dependent-gain controller quickly converges to

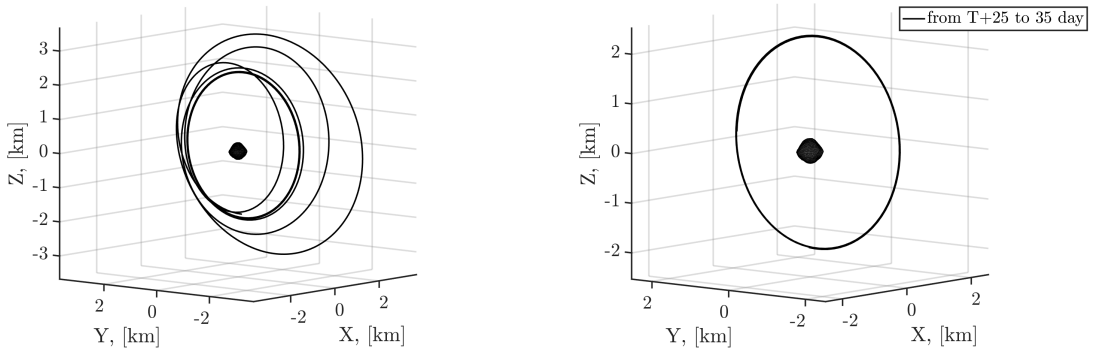

Figure 7. Spacecraft trajectory with stationkeeping control by SRP, with the state-dependent gain. Left: from the initial epoch to the end, right: last ten days (to emphasize the convergence). The same initial perturbation as in Figure 5 is added.

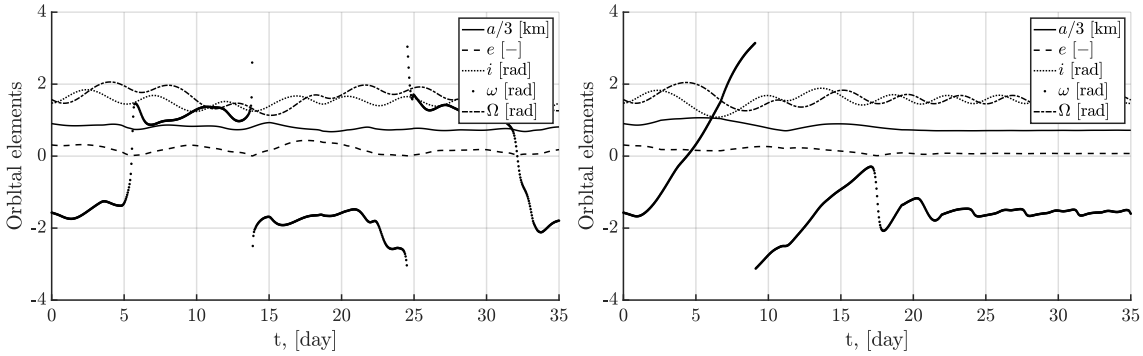

Figure 8. Time histories of osculating orbital elements, controlled by the SRP-based orbit control with the constant (left) and state-dependent (right) feedback gains. The right figure shows convergence of the orbital elements to the reference orbit (Figure 4).

the target orbit in a straightforward manner. Note that however the argument of the periapsis ω does not seem converging directly to the target value (crossing 0, starting from $\sim \pi/2$); figuring out the reason might require further investigation of the relationship between the results and the feedback gain. Also note that i, ω, and Ω are oscillating around the target values after convergence of a and e, which would be mainly due to disturbances caused by the irregular gravity field, solar gravity, and evolution of the asteroid around the Sun.

To compare the control inputs of the controllers, Figures 9 show time histories of attitude control inputs $\{\alpha, \beta\}$ for the stationkeeping control with the constant gain (left) and the state-dependent gain (right). Note that the pitch angle α is kept < 15 degree as specified in Table 2, and the clock angle β takes various values in $[-\pi, \pi]$. Although this simulation assumes that the attitude can be instantaneously changed, a certain attitude maneuverability constraint should be imposed to achieve such SRP-based orbit controls in practice. SRP-based orbit controls with the attitude maneuverability consideration would be future work.

Orbit transfer

As another application example, this subsection applies the SRP-based orbit control to orbit transfer scenarios. The Lyapunov feedback controller with the state-dependent gain is tested since it is

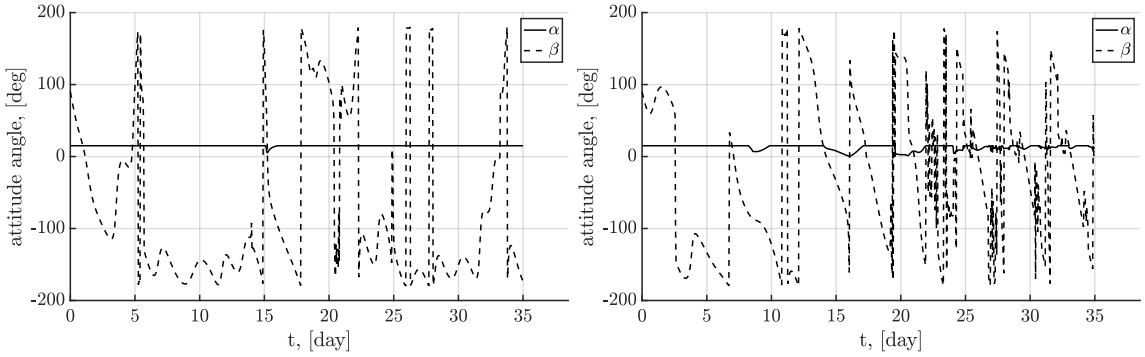

Figure 9. Time histories of attitude control inputs $\{\alpha, \beta\}$ for stationkeeping control with the constant (left) and state-dependent (right) feedback gains. The pitch angle α is kept less than 15 degree.

Table 4. Initial (A) and target (B) orbits for orbit transfer scenario. Spacecraft parameters similar to OSIRIS-REx and Hayabusa are assumed.

Spacecraft	a_{A}	e_{A}	i_{A}	ω_{A}	Ω_{A}	a_{B}	e_{B}	i_{B}	ω_{B}	Ω_{B}
OSIRIS-REx	1.5	0.0815	$\pi/2$	$-\pi/2$	$\pi/2$	1.0	0.0997	$\pi/2$	$-\pi/2$	$\pi/2$
Hayabusa	1.5	0.0342	$\pi/2$	$-\pi/2$	$\pi/2$	1.0	0.0419	$\pi/2$	$-\pi/2$	$\pi/2$

clear that the state-dependent-gain controller is superior to the constant-gain one. This subsection considers two types of spacecraft parameters to show the potential orbit control capability by SRP with different spacecraft parameters.

One of the two spacecraft parameters is the same as the one used in the simulations of the previous subsection, i.e., the one similar to the OSIRIS-REx spacecraft (Table 2). The other one assumes a slightly higher area-to-mass ratio, $\sigma = 1/31\ [\mathrm{m}^2/\mathrm{kg}]$, which is comparable to the Hayabusa spacecraft,[16] with keeping other parameters unchanged from the OSIRIS-REx ones. Let us emphasize that the maximum allowable pitch angle of the attitude control is kept to be < 15 degree.

The transfer scenario assumes that a spacecraft transfers from a higher-altitude science orbit to a lower one at Bennu. The scenario is inspired by the science planning of the OSIRIS-REx mission, where the spacecraft lowers its orbit from Orbit A to B.[15,26] The Orbit A and B are terminator orbits of 1.5 km and 1.0 km altitudes, respectively. As the science orbits A and B, this paper uses the frozen terminator orbits introduced in the "Frozen terminator orbit" subsection (note that, although the actual science orbits A and B will be terminator orbits, they will not be frozen ones). Following the discussion in the subsection, orbital elements of the initial (A) and target (B) orbits are calculated for each set of spacecraft parameters and summarized in Table 4. Even with the same orbit semi-major axis a, the orbit eccentricities e are different from each other depending on spacecraft parameters.

The transfer control results are shown in Figures 10 (OSIRIS-REx) and 11 (Hayabusa), where the left figures illustrate the spacecraft trajectories in the ACH frame and the right ones plot time histories of the osculating orbital elements. Note that the trajectories in Figures 10 and 11 are propagated for 35 days and for 20 days, respectively. The both cases successfully complete the transfers, and the target orbit is achieved with oscillations in i, ω, and Ω, which are the same phenomena as observed in the stationkeeping scenario. While the transfer with the OSIRIS-REx spacecraft pa-

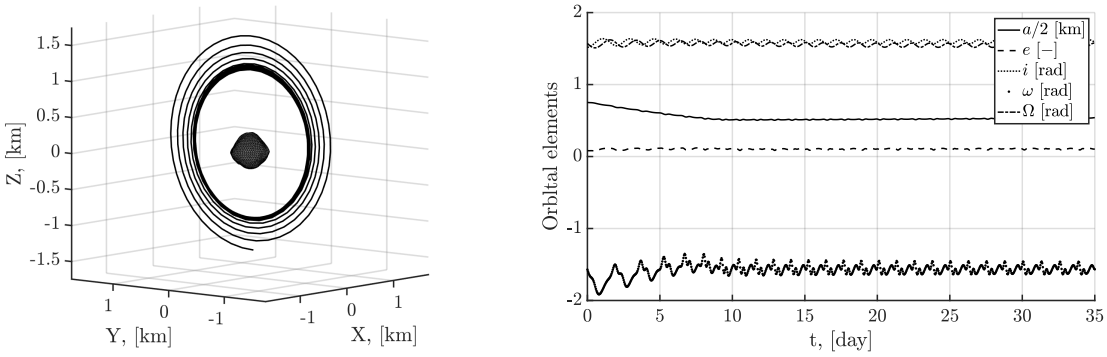

Figure 10. Orbit transfer by SRP from a 1.5 km frozen terminator orbit to a 1.0 km one (corresponding to OSIRIS-REx science orbits A and B). Spacecraft parameters similar to OSIRIS-REx are assumed. Lyapunov feedback control law with state dependent gains. Left: transfer trajectory, right: time history of osculating orbital elements. The transfer completes in 10 days.

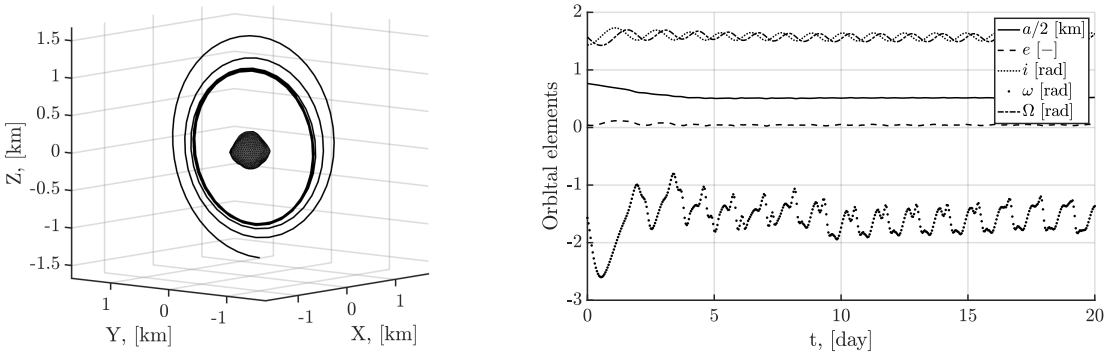

Figure 11. Orbit transfer by SRP from a 1.5 km frozen terminator orbit to a 1.0 km one (corresponding to OSIRIS-REx science orbits A and B), with area-to-mass ratio of $\sigma = 1/31\ [\mathrm{m}^2/\mathrm{kg}]$ (comparable to that of the Hayabusa spacecraft). Lyapunov feedback control law with state dependent gains. Left: transfer trajectory, right: time history of osculating orbital elements. The transfer completes in 5 days.

rameters spent 10 days complete the transfer, that with the Hayabusa parameters completed it in 5 days.

The comparison implies that the orbit control capability would be significantly improved with a slightly larger area-to-mass ratio. This observation could pose a suggestion for future spacecraft design approach to improve orbit control capability by utilizing SRP at small bodies.

Figures 12 visualize the transfer profiles in terms of a and e, overlaying them on a contour of the value of the Lyapunov function V (Eq. 10). They illustrate how each trajectory approaches to the target orbit under the SRP-based orbit control, governed by the state-dependent gain. Since each oscillation in the profiles corresponds to each orbit around the body, we qualitatively see from these figures that how many orbits are required to complete the transfer and how largely a and e are changed due to the control over each orbit.

As revealed in the two scenarios of this paper, a quantity of appropriately measuring the "distance" between osculating elements and target ones would be necessary to perform the SRP-based orbit control more efficiently in a highly perturbed environment. It would help evaluate convergence

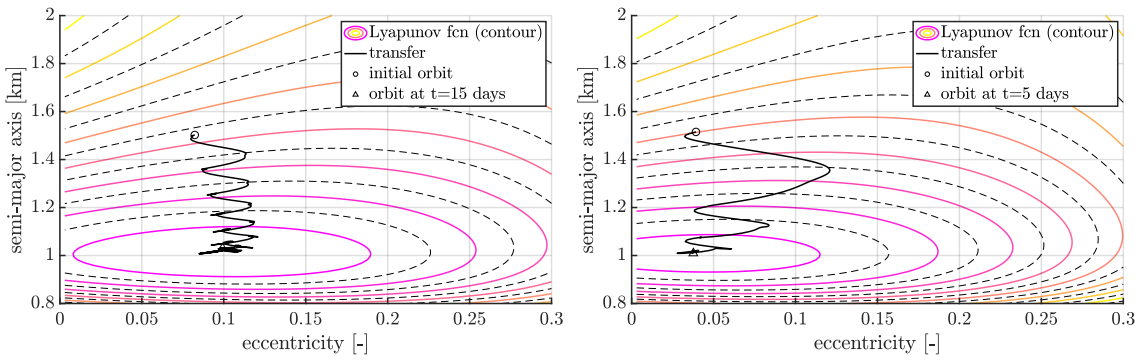

Figure 12. Orbit transfers expressed in terms of a and e, overlaid on contours of the Lyapunov function value V (defined in Eq. 10). Left and right figures correspond to transfer trajectories shown in Figures 10 and 11, respectively.

to target orbits and then terminate the orbit control with smooth convergence to the target.

CONCLUSIONS

This paper investigated the capability of the SRP-based orbit control at a small body environment by a common spacecraft (not with a large area-to-mass ratio like solar sails). A state-dependent feedback gain inspired by the Q-law is introduced to an optimal SRP-based orbit control law that was previously developed by the authors. We first applied the controller to an orbit stationkeeping scenario, where numerical simulations of stationkeeping control on frozen terminator orbits are performed assuming OSIRIS-REx-like spacecraft at Bennu with a maximum pitch angle constraint of < 15 deg, under disturbances of the irregular gravity field (16×16), solar gravity, and SRP. The simulations demonstrated that orbit stationkeeping via SRP is an available option at small body environments even with a common spacecraft with small attitude changes. The controller is also applied to an orbit transfer scenario inspired by the OSIRIS-REx science planning. Numerical simulations demonstrated that an orbit transfer from the OSIRIS-REx science orbit A to B could be achieved solely by SRP in 5 days by a spacecraft with a slightly higher area-to-mass ratio (comparable to the Hayabusa spacecraft). The two specific demonstrations would suggest a new orbit control option for future asteroid exploration missions: SRP-based orbit control.

ACKNOWLEDGMENT

The authors would like to thank NASA Innovative Advanced Concept (NIAC) program for funding this work. K. Oguri acknowledges financial support for his Ph.D. study from Nakajima Foundation and Masason Foundation. K. Oguri would also like to thank Gregory Lantoine and Anastassios Petropoulos at the Jet Propulsion Laboratory for some early discussions on the use of the Q-law as a state-dependent feedback gain for the SRP-based orbit control.

REFERENCES

[1] D. J. Scheeres, *Orbital Motion in Strongly Perturbed Environments: Applications to Asteroid, Comet and Planetary Satellite Orbiters*. Chichester, UK: Springer, 2012, 10.1007/978-3-642-03256-1.

[2] H. Dankowicz, "Some special orbits in the two-body problem with radiation pressure," *Celestial Mechanics & Dynamical Astronomy*, Vol. 58, No. 4, 1994, pp. 353–370.

[3] D. J. Scheeres, "Orbit Mechanics About Asteroids and Comets," *Journal of Guidance, Control, and Dynamics*, Vol. 35, No. 3, 2012, pp. 987–997.

[4] S. M. Byram and D. J. Scheeres, "Stability of Sun-Synchronous Orbits in the Vicinity of a Comet," *Journal of Guidance, Control, and Dynamics*, Vol. 32, No. 5, 2009, pp. 1550–1559.

[5] S. B. Broschart, G. Lantoine, and D. J. Grebow, "Quasi-terminator orbits near primitive bodies," *Celestial Mechanics and Dynamical Astronomy*, Vol. 120, No. 2, 2014, pp. 195–215.

[6] D. Lantukh, R. P. Russell, and S. B. Broschart, "Heliotropic orbits at oblate asteroids: Balancing solar pressure and j2 perturbations," *Celestial Mechanics and Dynamical Astronomy*, Vol. 121, 2015, pp. 171–190.

[7] R. P. Russell, D. Lantukh, and S. B. Broschart, "Heliotropic Orbits at Asteroids: Zonal Gravity Perturbations and Application at Bennu," *Journal of Guidance, Control, and Dynamics*, Vol. 39, No. 9, 2015.

[8] S. Kikuchi, Y. Tsuda, and J. Kawaguchi, "Delta-V assisted periodic orbits around small bodies," *Journal of Guidance, Control, and Dynamics*, Vol. 158, No. 1, 2016, pp. 3661–3680.

[9] E. Morrow, D. J. Scheeres, and D. Lubin, "Solar Sail Orbit Operations at Asteroids," *Journal of Spacecraft and Rockets*, Vol. 38, No. 2, 2001, pp. 279–286.

[10] G. Misra, M. Izadi, A. Sanyal, and D. J. Scheeres, "Coupled orbit-attitude dynamics and relative state estimation of spacecraft near small Solar System bodies," *Advances in Space Research*, Vol. 57, No. 8, 2016, pp. 1747–1761.

[11] X. Zeng, S. Gong, J. Li, and K. T. Alfriend, "Solar Sail Body-Fixed Hovering over Elongated Asteroids," *Journal of Guidance, Control, and Dynamics*, Vol. 39, No. 6, 2016, pp. 1–9, 10.2514/1.G001061.

[12] J. Heiligers and D. J. Scheeres, "Solar Sail Orbital Motion About Asteroids and Binary Asteroid Systems," *AAS/AIAA Space Flight Mechanics Meeting*, 2017.

[13] S. Kikuchi, K. C. Howell, Y. Tsuda, and J. Kawaguchi, "Orbit-attitude coupled motion around small bodies: Sun-synchronous orbits with Sun-tracking attitude motion," *Acta Astronautica*, Vol. 140, No. December 2016, 2017, pp. 34–48.

[14] K. Oguri and J. W. McMahon, "SRP-based Orbit Control with Application to Small Body Landing," *AAS/AIAA Astrodynamics Specialist Conference*, Snowbird, UT, 2018, pp. 1–19.

[15] D. S. Lauretta, S. S. Balram-Knutson, E. Beshore, W. V. Boynton, C. Drouet d'Aubigny, D. N. DellaGiustina, H. L. Enos, D. R. Golish, C. W. Hergenrother, E. S. Howell, C. A. Bennett, E. T. Morton, M. C. Nolan, B. Rizk, H. L. Roper, A. E. Bartels, B. J. Bos, J. P. Dworkin, D. E. Highsmith, D. A. Lorenz, L. F. Lim, R. Mink, M. C. Moreau, J. A. Nuth, D. C. Reuter, A. A. Simon, E. B. Bierhaus, B. H. Bryan, R. Ballouz, O. S. Barnouin, R. P. Binzel, W. F. Bottke, V. E. Hamilton, K. J. Walsh, S. R. Chesley, P. R. Christensen, B. E. Clark, H. C. Connolly, M. K. Crombie, M. G. Daly, J. P. Emery, T. J. McCoy, J. W. McMahon, D. J. Scheeres, S. Messenger, K. Nakamura-Messenger, K. Righter, and S. A. Sandford, "OSIRIS-REx: Sample Return from Asteroid (101955) Bennu," *Space Science Reviews*, Vol. 212, No. 1-2, 2017, pp. 925–984, 10.1007/s11214-017-0405-1.

[16] J. Kawaguchi, A. Fujiwara, and T. Uesugi, "Hayabusa-Its technology and science accomplishment summary and Hayabusa-2," *Acta Astronautica*, Vol. 62, No. 10-11, 2008, pp. 639–647, 10.1016/j.actaastro.2008.01.028.

[17] A. E. Petropoulos, "Simple control laws for low-thrust orbit transfers," *Advances in the Astronautical Sciences*, Vol. 99, No. 2, 2003, pp. 1455–1468.

[18] A. E. Petropoulos, "Low-Thrust Orbit Transfers Using Candidate Lyapunov Functions with a Mechanism for Coasting," *AIAA/AAS Astrodynamics Specialist Conference*, 2004.

[19] A. E. Petropoulos, "Refinements to the Q-law for low-thrust orbit transfers," *Advances in the Astronautical Sciences*, Vol. 120, No. I, 2005, pp. 963–982.

[20] C. R. McInnes, "Artificial Lagrange points for a partially reflecting flat solar sail," *Journal of guidance, control, and dynamics*, 1999.

[21] L. Rios-Reyes and D. J. Scheeres, "Generalized Model for Solar Sails," *Journal of Spacecraft and Rockets*, Vol. 42, No. 1, 2005, pp. 182–185, 10.2514/1.9054.

[22] L. Rios-Reyes and D. J. Scheeres, "Solar-Sail Navigation: Estimation of Force, Moments, and Optical Parameters," *Journal of Guidance, Control, and Dynamics*, Vol. 30, may 2007, pp. 660–668, 10.2514/1.24340.

[23] D. A. Vallado, *Fundamentals of astrodynamics and applications*. Springer Science & Business Media, 12 ed., 2001.

[24] D. J. Scheeres, S. G. Hesar, S. Tardivel, M. Hirabayashi, D. Farnocchia, J. W. Mcmahon, S. R. Chesley, O. Barnouin, R. P. Binzel, W. F. Bottke, M. G. Daly, J. P. Emery, C. W. Hergenrother, D. S. Lauretta, J. R. Marshall, P. Michel, M. C. Nolan, and K. J. Walsh, "The geophysical environment of Bennu," *Icarus*, Vol. 276, 2016, pp. 116–140.

[25] S. Takahashi and D. J. Scheeres, "Effect of Shifted Origin on the Osculating Orbital Elements of Terminator Orbit," *29th AAS/AIAA Space Flight Mechanics Meeting*, Maui, HI, 2019.

[26] B. Williams, P. Antreasian, E. Carranza, C. Jackman, J. Leonard, D. Nelson, B. Page, D. Stanbridge, D. Wibben, K. Williams, M. Moreau, K. Berry, K. Getzandanner, A. Liounis, A. Mashiku, D. Highsmith, B. Sutter, and D. S. Lauretta, *OSIRIS-REx Flight Dynamics and Navigation Design*, Vol. 214. Springer Science+Business Media B.V., part of Springer Nature, 2018, 10.1007/s11214-018-0501-x.

[27] S. G. Hesar, D. J. Scheeres, and J. W. McMahon, "Sensitivity Analysis of the OSIRIS-REx Terminator Orbits to Maneuver Errors," *Journal of Guidance, Control, and Dynamics*, Vol. 156, No. 1, 2016, pp. 3747–3766, 10.2514/1.G002058.